J. Fluid Mech. (1986), *vol.* 165, *pp.* 401–424
Printed in Great Britain

Structure of the temperature field downwind of a line source in grid turbulence

By H. STAPOUNTZIS†
Department of Engineering, University of Cambridge, Cambridge CB2 1PZ

B. L. SAWFORD,
CSIRO, Division of Atmospheric Research, Private Bag No. 1, Mordialloc, Victoria, 3195, Australia

J. C. R. HUNT‡
Department of Applied Mathematics and Theoretical Physics, University of Cambridge, Cambridge CB3 9EW

AND R. E. BRITTER
Department of Engineering, University of Cambridge, Cambridge CB2 1PZ

(Received 8 June 1983 and in revised form 10 June 1985)

A Lagrangian stochastic model is used in conjunction with detailed wind-tunnel measurements to examine the structure and development of the temperature field behind a line source in grid turbulence. It is shown that on the scale of these experiments molecular diffusion and viscosity have an important influence on temperature fluctuations (particularly on the intensity of these fluctuations) and must be explicitly modelled. The model accounts for a wide range of the measured properties of the temperature field and provides a unified treatment of temperature fluctuations through all stages of the development of the temperature field. This development is discussed in terms of a simple physical picture in which the hot plume is initially smooth and is moved about bodily by the turbulence, but gradually develops increasing internal structure or patchiness as it grows with distance downstream until a self-similar state is reached in which this internal structure maintains the temperature fluctuations.

1. Introduction

Casual observations of meandering chimney plumes show that there are pockets of clear air amongst the smoke and casual sniffing of the air downwind of smelly sources shows how intermittent is the concentration of contaminant even many kilometres downwind. These simple observations reflect the fact that as a contaminant disperses from a source in a turbulent flow, it is wafted around in a narrow 'plume' within which there are large fluctuations in concentration and that, even when the plume has grown so wide that it no longer appears to be meandering, there are still large fluctuations in concentration due to this internal structure. These phenomena can also be clearly seen in the temperature traces downwind of a heated wire in a turbulent flow in a wind tunnel (Uberoi & Corrsin 1953), in a wind-tunnel smoke plume (especially seen from downwind (Hunt 1976)), and in recent fast-response plume measurements in the atmosphere (Jones 1982).

† Present address: University of Thessaloniki, Box 443, Greece 54006.
‡ Also Department of Engineering.

Theories for the fluctuating concentrations in plumes have mainly concentrated on the meandering of the plume and have failed to account for the growth of fluctuations within the meandering plume (e.g. Uberoi & Corrsin 1953; Gifford 1960; Fackrell & Robins 1982). Such theories provide useful estimates for the variance of concentration or temperature, $\overline{\theta'^2}$ or σ_θ^2, in the initial stages of the plume's growth but are quantitatively and qualitatively in error later on (Sawford 1983). On the other hand, the asymptotic stage of the concentration fluctuations in continuous plumes has been described in terms of self-similar profiles but not predicted theoretically (Csanady 1973, ch. 7). This approach, which relies on K-theory to represent spatial transfer processes, and on models for the decay of variance, cannot represent the initial, meander-dominated stage of the development of concentration fluctuations.

This paper describes a theoretical, computational and experimental investigation into these well-known aspects of turbulent diffusion for which a proper qualitative understanding and good quantitative estimates are at present lacking. The theory is based on the marked-particle models of Lamb (1981), Durbin (1980) and Sawford (1983) and provides a unified treatment of all stages of the development and decay of concentration fluctuations in a plume.

The extension of Durbin's (1980) model to low-Reynolds-number turbulence was developed and explored in detail for stationary homogeneous turbulence by Sawford & Hunt (1986) [hereinafter referred to as SH]. In the present paper we describe an experiment and specific computations for decaying homogeneous turbulence. We measured fluctuating temperatures downstream of a heated wire in grid-generated turbulence in a wind tunnel. The aspects of this experiment that are different to those performed by Uberoi & Corrsin (1953), Townsend (1954), Warhaft (1984) and others were that we measured the turbulence in some detail and also the temperature field from very close to the wire to 80 grid mesh-lengths downwind. These measurements were necessary in order to calculate the mean and fluctuating temperature in terms of the initial conditions at the source and the turbulence by using the random-walk computations described in SH. Where possible our temperature and turbulence measurements have been compared with those in other experiments. The relatively low Reynolds number of these experiments, although a complication, shows up very clearly the roles of molecular diffusion and source size.

Recently, there have been a number of experiments (Warhaft & Lumley 1978; Sreenivasan *et al.* 1980) using groups of variously heated wires in grid turbulence in order to generate various profiles of mean and fluctuating temperature. These experiments have generally been interpreted in terms of the distribution of temperature rather than in terms of the 'plumes' from individual wires. For example, Durbin (1982) treated the temperature distribution of an array of wires as a random initial temperature field. One of the aims of our experiment and the computations is to show that most of the features of the temperature field produced by a single wire can be understood and computed. It may then be interesting to compute the aggregate fields of several wires (Warhaft 1984 has already applied this approach experimentally) and to compare the results with calculations based on a random initial temperature field. There are likely to be differences in the results because such calculations have to *assume* certain statistical properties of the initial random temperature field which are in fact determined by the turbulent flow passing the heated wires.

It is also relevant to note the connection between the growth and decay of temperature fluctuations and mixing and reaction of chemical species in turbulence. Normally this parallel is drawn when considering models based on moments of

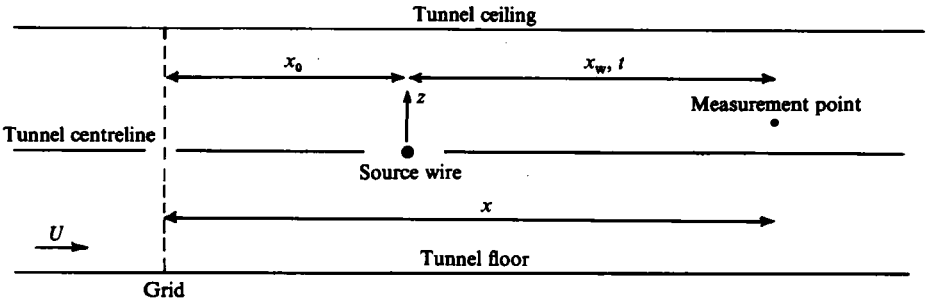

FIGURE 1. Schematic wind-tunnel layout.

velocity, concentration or chemical species (e.g. Bray 1980). However, Durbin's theoretical model, developed in SH and applied here, shows that the decay of temperature fluctuations is largely caused by mixing of two fluid elements originating from regions of different initial temperature. This process, which can be studied fairly precisely in the decay of fluctuations of scalar contaminants, is also the basis for the mixing of chemical species and is modelled (with somewhat less emphasis of the fluid mechanics) in many *statistical* models of chemical reactions and combustion in turbulent flow (Pope 1979).

2. Measurements

2.1. *Experimental set-up*

The experiments were conducted in a suction wind tunnel with a rectangular test section 0.508 m high, 0.191 m wide and 3.2 m long. The experimental set-up is shown in figure 1. The turbulence was generated by a biplanar grid of mesh size $M = 2.54 \times 10^{-2}$ m (1 in.) and solidity ratio 0.47. Temperature fluctuations were produced by a heated Nichrome wire placed a distance $x_0 = 19.3\,M$ downstream of the grid and spanwise across the centre of the tunnel. It was kept taut by means of springs placed outside the working section. The experiments were carried out with a mean air speed $U = 4.35$ m s^{-1}. The flow Reynolds number based on M, $Re_M = UM/\nu$, was 6.8×10^3 where ν is the kinematic viscosity of the unheated air (1.62×10^{-5} m^2 s^{-1} at 30 °C).

For most of the temperature measurements a wire of diameter $d_w = 1.52 \times 10^{-4}$ m was used in order to achieve a wire Reynolds number, $Re_w = Ud_w/\nu$, low enough to avoid vortex shedding. At room temperature, Re_w for this wire was about 40, but as pointed out by Uberoi & Corrsin (1953), this value is reduced considerably by the increased viscosity of the air near the heated wire. Some measurements were also done with a thicker wire ($d_w = 7.71 \times 10^{-4}$ m; Re_w about 200 at room temperature) in order to examine the effect of vortex shedding on the temperature field.

Streamwise velocity fluctuations were measured with a tungsten hot-wire of diameter 5 μm and length 1.25 mm powered by a DISA 55M01 constant-temperature anemometer circuit. The transverse components were measured with a crossed hot-wire probe using similar tungsten wires. Temperature fluctuations were measured with a platinum cold wire 1 μm in diameter and 0.4 mm long supplied with a constant current of 0.3 mA using a temperature bridge in conjunction with a 55M01 anemometer. The length of this cold-wire is comparable with the Kolmogorov lengthscale, $\eta = (\nu^3/\epsilon)^{\frac{1}{4}}$, for our experiments (the rate of dissipation of energy ϵ is given by (2.5) below). Thus according to Wyngaard (1971), it responds to over 90 % of the

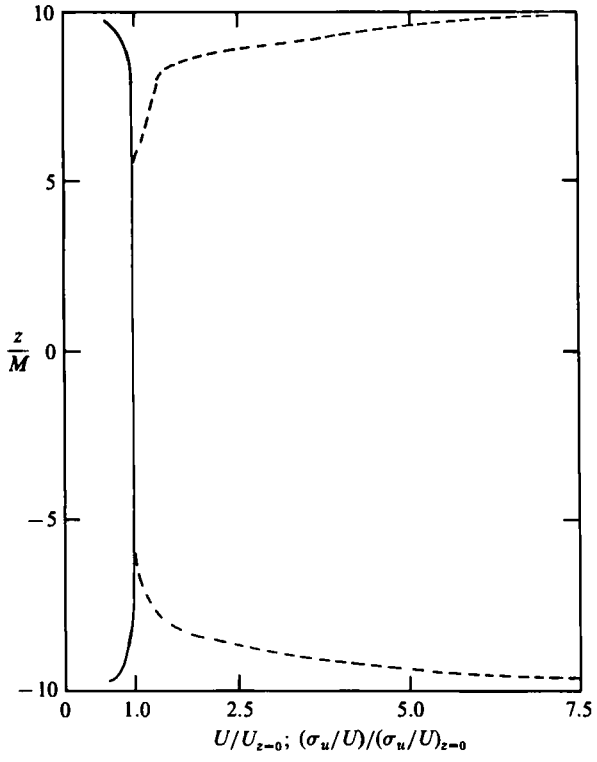

FIGURE 2. Transverse homogeneity of mean wind speed (——) and intensity of longitudinal component of turbulence (– – – –).

temperature variance. Mean temperatures were measured relative to a reference point upstream of the source using a pair of copper–constantan thermocouples, the difference in output being fed to an integrating voltmeter set to 100 s integration time. The effect of variations in room temperature on temperature measurements in the tunnel was reduced to ± 0.02 °C by premixing the air entering the tunnel with a blower.

2.2. *Properties of the turbulence*

Figure 2 shows the transverse homogeneity of the mean free-stream speed, U, and the longitudinal turbulent velocity u. The tunnel-wall boundary layers were quite thick towards the end of the working section, limiting the region of 'homogeneous turbulence' to about $\pm 7M$ from the tunnel centreline. This was an acceptable limitation.

The decay of the turbulent velocity fluctuations is shown in figure 3. Note that σ_w is lower that σ_u, this anisotropy being partly a result of the size of the cross-section. The decay rates for σ_u from other work are also shown for a comparison. For the present data we have

$$\sigma_u^2/U^2 = 0.22\left(\frac{x}{M}\right)^{-1.42} \tag{2.1}$$

and

$$\sigma_w^2/U^2 = 0.15\left(\frac{x}{M}\right)^{-1.43} \tag{2.2}$$

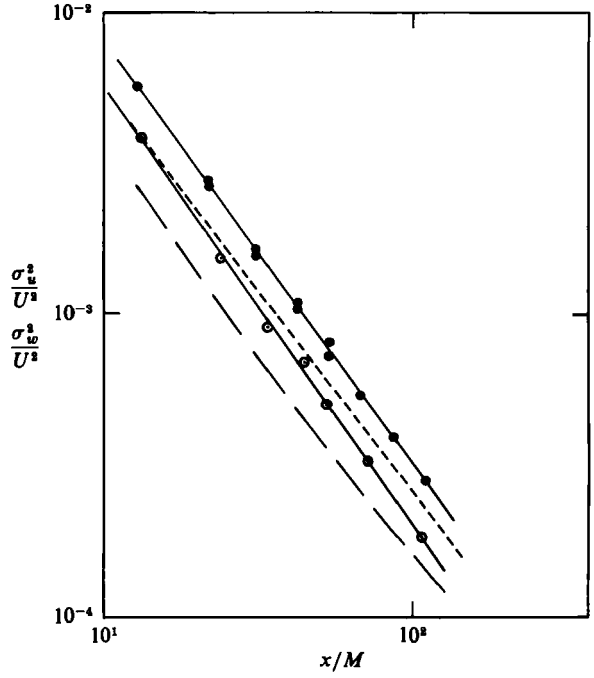

FIGURE 3. Decay of turbulence velocity fluctuations. Longitudinal components: present experiments (●); Warhaft & Lumley (1978) (---); Sreenivasan *et al.* (1980) (——). Vertical component: present experiments (⊙).

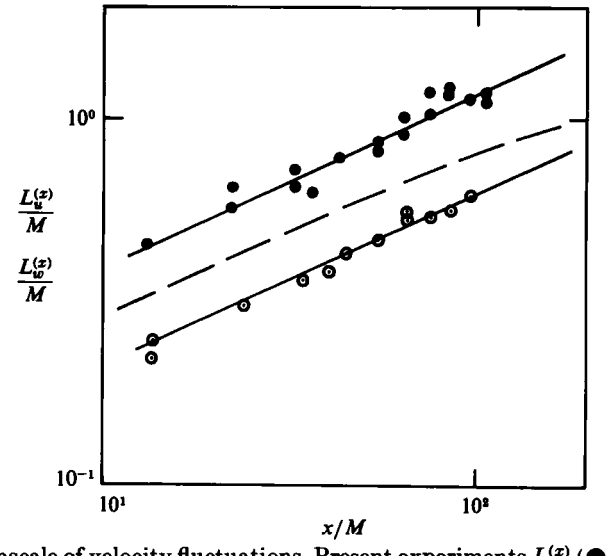

FIGURE 4. Lengthscale of velocity fluctuations. Present experiments $L_u^{(x)}$ (●), $L_w^{(x)}$ (⊙). Sreenivasan *et al.* (1980): $L_u^{(x)}$ (——).

Only the variation of w with distance from the source is needed in the random-walk calculations.

Figure 4 shows the integral length scales of the u and w fluctuations. These were estimated both from frequency spectra (assuming Taylor's hypothesis and a 'von Kármán' spectral shape) and from time correlations (assuming Taylor's hypothesis)

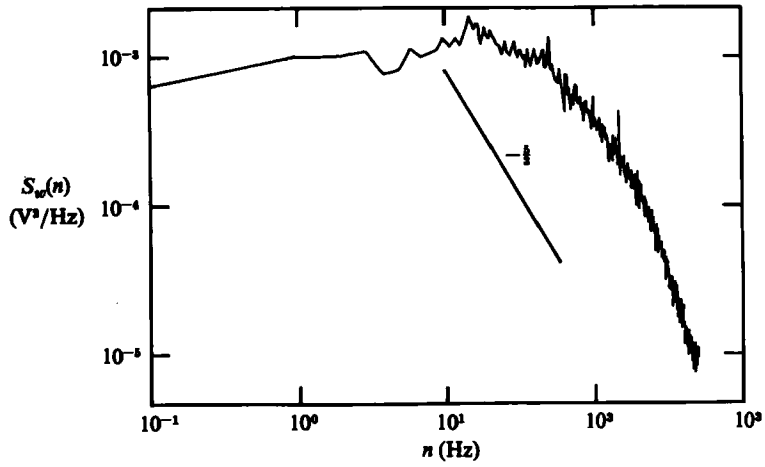

FIGURE 5. Spectrum of vertical velocity fluctuations at $x/M = 85$.

and are in good agreement with those of other workers. Again, only the transverse lengthscale is used in the random-walk calculations, and is given by

$$L_w^{(x)}/M = 7.03 \times 10^{-2} \left(\frac{x}{M}\right)^{0.47}. \tag{2.3}$$

As is well recognized (Hinze 1975, ch. 3), the turbulence is not quite self-preserving in this initial stage of decay, and the Reynolds number of the turbulence, $Re = \sigma_w L_w^{(x)}/\nu$, varies weakly with distance downstream,

$$Re = 1.86 \times 10^2 \left(\frac{x}{M}\right)^{-0.25}. \tag{2.4}$$

Over the range of our measurements, $x/M = 19.3$ to 85, Re varies from 90 to 63.

Figure 5 shows the velocity spectrum for the transverse component at $x/M = 85$. As might be expected for such low-Reynolds-number turbulence, there is no appreciable inertial range.

The rate of dissipation of energy has been calculated as

$$\epsilon = -\tfrac{3}{2}\mathrm{d}\sigma_u^2/\mathrm{d}t = -\tfrac{3}{2}U\mathrm{d}\sigma_u^2/\mathrm{d}x$$

so from (2.1) we have

$$\epsilon = 4.69 \times 10^{-1} \frac{U^3}{M}\left(\frac{x}{M}\right)^{-2.42}. \tag{2.5}$$

Note that the ratio $\sigma_w^3/L_w^{(x)}\epsilon$ is only weakly dependent on $x(\approx x^{-0.2})$ and varies only from 0.98 to 0.75 for x/M between 19.3 and 85.

3. Theory

3.1. *Outline of the model*

We use a Lagrangian statistical model (a 'random-walk' model) to calculate the mean $\bar{\theta}$ and mean-square $\overline{\theta^2}$ concentration of a scalar quantity from the probability distribution of the displacements of independent molecules and independent molecule-pairs and from the source distribution of the scalar. The continuous line source in

which we are interested can be approximated by an instantaneous plane source using the Taylor transformation $x = Ut$ provided that the streamwise velocity fluctuations are small compared with the mean flow. Then $\bar{\theta}$ and $\overline{\theta^2}$ are given by (Batchelor 1952; Monin & Yaglom 1971; SH)

$$\bar{\theta}(z, t) = \int_{-\infty}^{\infty} P_1(z', 0; z, t)\, S(z')\, \mathrm{d}z', \tag{3.1}$$

and

$$\overline{\theta^2}(z, t) = \int\int_{-\infty}^{\infty} P_2(z_1', z_2', 0; z, z, t)\, S(z_1')\, S(z_2')\, \mathrm{d}z_1'\, \mathrm{d}z_2', \tag{3.2}$$

where $S(z')$ is the initial source distribution. P_1 and P_2 are probability density functions (p.d.f.'s) for the displacement of single molecules and pairs of molecules respectively. Note that Durbin's (1980) model (and the extension we use here) treats only the z-component of the trajectories and therefore cannot satisfy the incompressibility constraint. Sawford (1984) and SH show that spurious effects of compressibility can be compensated for by using a reversed diffusion procedure (Corrsin 1952) in which $\bar{\theta}$ and $\overline{\theta^2}$ are calculated in mass-specific form from the dispersion of molecules backwards in time from the measurement point z to points within the source distribution. Our notation in (3.1) and (3.2) emphasizes this reversed diffusion process.

Our model consists of a prescription for generating realistic molecular trajectories under the joint influence of molecular and turbulent motions and is an extension of the model developed by Durbin (1980) for the motion of pairs of marked fluid elements. The physical basis for the model is discussed in detail in SH. Here we merely present the stochastic equations of motion for a pair of molecules. Written in centre-of-mass and separation variable, $\Sigma = (z_1+z_2)/\sqrt{2}$, and $\Delta = (z_1-z_2)/\sqrt{2}$ respectively, these are

$$\frac{\mathrm{d}\Delta}{\mathrm{d}t} = R^{\frac{1}{2}}(\Delta)\, U' + \sqrt{2\kappa}\, \frac{\mathrm{d}W_{\mathrm{d}}'}{\mathrm{d}t} \tag{3.3}$$

and

$$\frac{\mathrm{d}\Sigma}{\mathrm{d}t} = [2-R(\Delta)]^{\frac{1}{2}}\, U'' + \sqrt{(2\kappa)}\, \frac{\mathrm{d}W_{\mathrm{d}}''}{\mathrm{d}t} \tag{3.4}$$

where κ is the molecular diffusivity and the structure function $R(\Delta)$ for the turbulent velocities at two points separated by a distance $\sqrt{2}\Delta$ is given by

$$R(\Delta) = \left(\frac{\Delta^2}{\eta^2/\alpha^3+\Delta^2}\right)^{\frac{2}{3}} \left(\frac{\Delta^2}{L^2+\Delta^2}\right)^{\frac{1}{3}}, \tag{3.5}$$

which is an interpolation between the limiting cases $\Delta \ll \eta$, $\eta \ll \Delta \ll L$ and $\Delta \gg L$ where $L = L_w^{(x)}$. Here $\alpha^2 = \frac{2}{15}$. Thus (3.5) incorporates the form of the structure function in these limits of Δ lying in the Kolmogorov microscale (η), in the inertial subrange and over distances large compared with the large eddies, and we are modelling the effects of the spatial structure of the turbulence on the statistics of the motion of the pair of molecules.

U' and U'' are independent random velocities which incorporate the effect of 'memory' in the motions of the molecules. In the non-stationary conditions of decaying grid turbulence they are modelled by the Langevin equation

$$\mathrm{d}\left(\frac{U'}{\sigma_w}\right) = -\left(\frac{U'}{\sigma_w t_{\mathrm{L}}}\right) \mathrm{d}t + \left(\frac{2}{t_{\mathrm{L}}}\right)^{\frac{1}{2}} \mathrm{d}W_t'. \tag{3.6}$$

where t_L is the Lagrangian integral timescale and is well represented by L/σ_w in grid turbulence (Snyder & Lumley 1971). P. A. Durbin (private communication) has pointed out that it is important to consider changes in U'/σ_w rather than U' itself, in order that $\overline{U'^2}\ (t) = \sigma_w^2(t)$. In stationary turbulence (3.6) is equivalent to the assumption of an exponentially decaying Lagrangian correlation function which gives a (-2) inertial range in the Lagrangian spectrum of velocity fluctuations in agreement with Kolmogorov's similarity theory (Monin & Yaglom 1975, p. 361).

Molecular diffusion is represented by the white-noise processes $\mathrm{d}W'_\mathrm{d}$, $\mathrm{d}W''_\mathrm{d}$. SH point out that (3.3) includes interaction between the turbulent velocity field and molecular diffusion. Comparison with Saffman's (1960) result for diffusion of a spot of contaminant at small times (the only case where an exact result has been obtained) shows that with $\alpha^2 = \frac{2}{15}$ (3.3) correctly predicts the enhanced diffusion which results from the interaction between molecular diffusion and the straining effect of the turbulence on small scales.

In all the calculations presented below we approximate the source by a Gaussian form

$$S(z) = \frac{Q}{(2\pi)^{\frac{1}{2}}\sigma_0}\exp\left(-\frac{z^2}{2\sigma_0^2}\right), \tag{3.7}$$

where Q is the source strength. Then, since P_1 is Gaussian, the mean-field is given from (3.1) and (3.7) by

$$\bar{\theta}(z,t) = \frac{Q}{(2\pi)^{\frac{1}{2}}(\sigma_0^2+\sigma_z^2)^{\frac{1}{2}}}\exp\left(\frac{-z^2}{2(\sigma_0^2+\sigma_z^2)}\right), \tag{3.8}$$

where $\sigma_z^2(t)$ is the dispersion at the source of those molecules which pass through the measurement point z at time t.

Furthermore it is clear from (3.4) that Σ is only weakly dependent on Δ so that $P_2(z_1', z_2', 0; z, z, t) \approx P(\Sigma', 0; \Sigma, t)\, P(\Delta', 0; 0, t)$ and $P(\Sigma', 0; \Sigma, t)$ is almost Gaussian, where $P(\Sigma', 0; \Sigma, t)$ and $P(\Delta', 0; \Delta, t)$ are the centre-of-mass and separation p.d.f.s respectively. Then from (SH)

$$\overline{\theta^2}(z,t) = \frac{Q^2}{(2\pi)^{\frac{1}{2}}(\sigma_0^2+\sigma_\Sigma^2)^{\frac{1}{2}}}\exp\left(-\frac{z^2}{\sigma_0^2+\sigma_\Sigma^2}\right)\int_{-\infty}^{\infty} P(\Delta', 0; 0, t)\, S(\Delta')\,\mathrm{d}\Delta', \tag{3.9}$$

where $\sigma_\Delta^2 = (1-\rho)\sigma_z^2$ and $\sigma_\Sigma^2 = (1+\rho)\,\sigma_z^2$ are the dispersion at the source of the 'separation' and 'centre of mass' of pairs which pass through the measurement point at time t, and ρ is the correlation between the positions of these pairs. Thus according to our model, $\bar{\theta}$ and $\overline{\theta^2}$ are both Gaussian functions of position, but in general the fluctuation field $\overline{\theta'^2}\,(z,t) = \overline{\theta^2} - \bar{\theta}^2 = \sigma_\theta^2$ is not, nor does it generally have, a self-similar form, since the dispersions of the $\overline{\theta^2}$ and $\bar{\theta}^2$ fields are different. The result (3.9) also shows how $\overline{\theta^2}$ depends on the size of the source and that only pairs with separations comparable with the source size contribute to $\overline{\theta^2}$.

3.2. *Numerical method*

Integration of finite-difference forms of (3.3), (3.4) and (3.6) is straightforward and gives the random trajectories of the pair of molecules commencing at (z, t) and ending at the random points z_1' and z_2' at the source at time 0. The time step is chosen to resolve the appropriate details of the motion (see SH for details). Statistics are compiled over a large number (typically 10^4) of independent pairs.

Calculation of the dispersion statistics σ_z, σ_Δ, and σ_Σ is straightforward. Concentration statistics can be calculated as outlined by Durbin (1980) by averaging $S(z_1')\,S(z_2')$ and $\frac{1}{2}(S(z_1')+S(z_2'))$ over all pairs to give $\overline{\theta^2}$ and $\bar{\theta}$ respectively. However,

for discrete sources such as we consider here, the statistical uncertainty in these calculations increases with time, since as σ_z increases fewer and fewer molecules pass through the source. This problem can be reduced considerably by:

(*a*) calculating $\bar{\theta}$ from (3.8) using the numerical estimate for σ_z; and

(*b*) calculating $\int P(\Delta', 0; 0, t)\, S(\Delta')\, \mathrm{d}\Delta'$ as the average of $S(\Delta')$ over all pairs and then using the estimate for σ_z in (3.9) to calculate $\overline{\theta^2}\ (z, t)$.

The statistical uncertainties in θ and θ^2 are then $O(N_0^{-\frac{1}{2}})$ and $O(N_t^{-\frac{1}{2}})$ where N_0 is the total number of pairs and N_t is the number of pairs for which $|\Delta| \leqq \sigma_0$ at the source. The quantity of most interest is the fluctuation variance σ_θ^2 which is calculated as the difference $\overline{\theta^2} - \bar{\theta}^2$ so that the uncertainty in σ_θ^2 can be large when σ_θ^2 is small (for example, for large sources or very close to the source on the centreline or far from the source).

3.3. *Contribution to concentration fluctuations by meandering*

Sawford (1983) has shown that, for sufficiently small times, fluctuations are produced mainly by bulk movement of the cloud or plume as a whole (meandering). The meandering contribution to the mean-square temperature is (Sawford 1983).

$$\overline{\theta_M^2}(z, t) = \frac{Q^2}{(2\pi)\,(\sigma_r^2 + 2\sigma_c^2)^{\frac{1}{2}}\,\sigma_r} \exp\left[-\frac{z^2}{(\sigma_r^2 + 2\sigma_c^2)}\right]. \tag{3.10}$$

where $\sigma_r^2(t)$ is the ensemble-mean variance about the centre-of-mass of the positions of all the particles which pass through the source at time 0, i.e. it is the mean instantaneous variance of all particles in the plume at $x = Ut$. σ_c^2 is the variance of the centre-of-mass of all these particles. For a small source, $\sigma_0 \ll L$, we have

$$\left.\begin{aligned} \sigma_r^2 &\cong \sigma_0^2 + \sigma_\Delta^2, \\ \sigma_c^2 &\cong \sigma_z^2 - \sigma_\Delta^2. \end{aligned}\right\} \tag{3.11}$$

4. Experimental results and model comparison

4.1. *Estimation of effective source size*

The effective source size is determined by the thickness of the thermal boundary layer l_b around the hot wire, which, while related to the actual wire diameter, is unlikely to be exactly $\frac{1}{2}d_w$. Because of the low value of Re_w, the boundary layer can be treated as laminar. Then calculations based on Schlichting (1968, p. 294) give $l_b \cong 0.75\, d_w$ at $Re_w = 15$ and $1.25\, d_w$ at $Re_w = 5$. We have chosen $\sigma_0 = 0.92\, d_w$ to fit the observed spread of the mean plume close to the source ($x_w/M \leqq 0.3$). Because of the dominance of molecular diffusion in this laminar boundary layer, the assumed Gaussian source distribution (3.8) is likely to be a reasonable approximation.

4.2. *Vertical profiles*

Figure 6 shows the vertical distribution of $\bar{\theta}$ and $\overline{\theta^2}$ for a range of downstream positions. Although there is some scatter, the data are well represented by Gaussian curves in agreement with the model predictions (3.8) and (3.9).

Figure 7 shows observed (from the fitted Gaussian curves) and predicted (from (3.8) and (3.9)) widths of the mean and mean-square fields σ_m and σ_s respectively as functions of x_w. Both are well represented by the model, although again there is considerable scatter in the data. Very close to the source, both σ_m and σ_s are strongly influenced by the source size, asymptoting to σ_0 and $\frac{1}{\sqrt{2}}\sigma_0$ respectively in agreement with the theoretical predictions (3.8) and (3.9). It is difficult to discern a $t^{\frac{1}{2}}$ diffusive

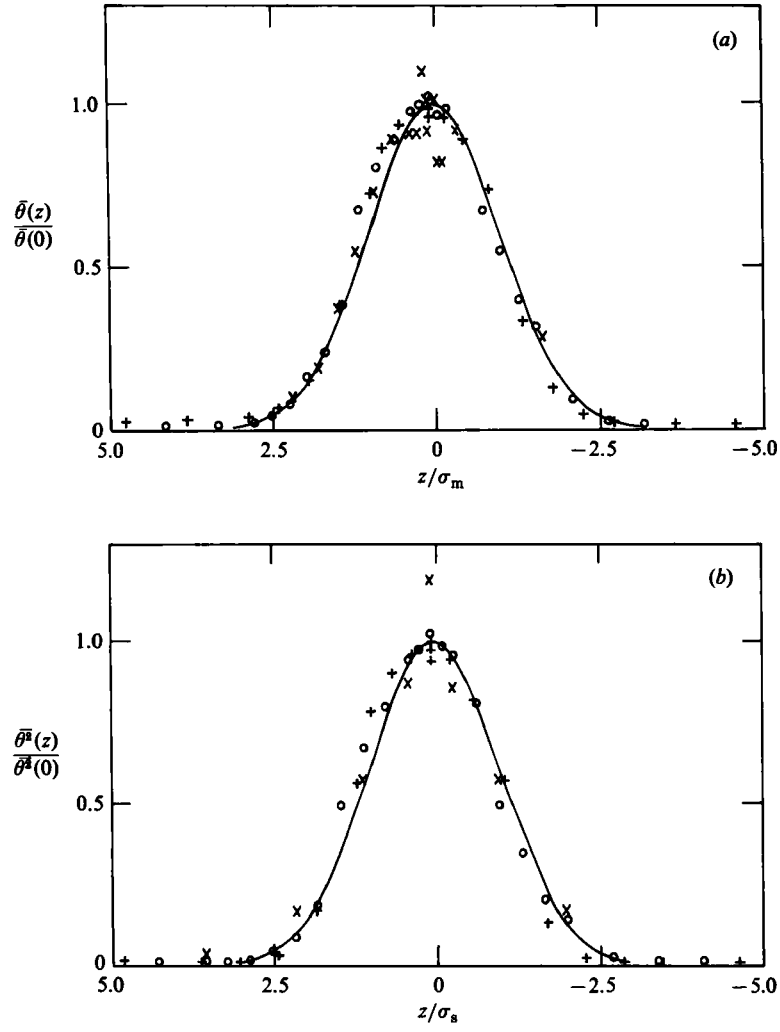

FIGURE 6. Vertical distribution of (*a*) mean temperature, and (*b*) mean-square temperature. Symbols are: +, $x_w/M = 3.9 \times 10^{-2}$; ○, x 2.0×10^{-1}; (×), 9.7.

growth range because of the finite source effect and also because the effective diffusivity is not constant but decreases significantly as the plume grows and cools. For $t_L(x_0) \gg t \gg \sigma_0/\sigma_w(x_0)$, σ_m grows nearly linearly with time, as predicted by Taylor's (1921) statistical theory. For large travel time ($t \gg t_L(x_0)$), Taylor's theory predicts $\sigma_m \sim x_w^{\frac{1}{2}}$ for stationary homogeneous turbulence. In turbulence for which $\sigma_w \sim x^{\mu-1}$; $L_w^{(x)} \sim x^\mu$ and $t_L \sim x$ the self-similar growth law, $\sigma_m \sim x_w^\mu$ applies for $t \gg t_L(0)$. Our turbulence data are reasonably well represented by $\mu = 0.4$ and we expect asymptotically that $\sigma_m \sim x^{0.4}$. There is too much scatter in the experimental data to confirm such a growth rate and in any case our data barely extend far enough downstream to satisfy the condition $t \gg t_L(x_0)$. Nevertheless, the model results are consistent with this theoretical asymptote.

Also shown as dashed lines in figure 7 are σ_m and σ_s calculated from Durbin's (1980) model for the motion of marked fluid elements, i.e. ignoring molecular diffusion and viscosity. These estimates clearly do not represent the data as well close to the source,

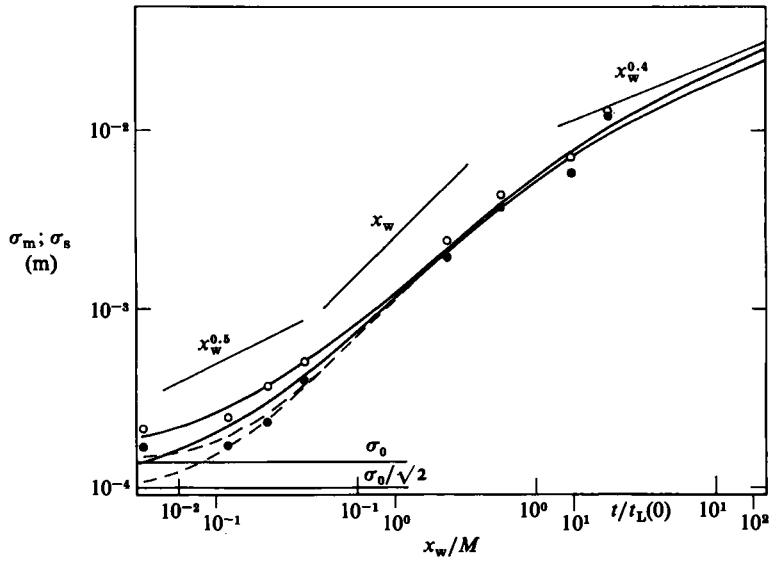

FIGURE 7. Dispersion σ_m and σ_s of mean and mean-square temperature distributions. Experiment: ⊙, σ_m ●, σ_s. Model: with molecular diffusion and viscosity (—); without molecular effects (– –); in both cases upper curves are for σ_m.

but further downstream the effect of molecular processes on the width of the mean and mean-square fields is of the order of Pe^{-1} (or $\kappa/(\sigma_w L)$) (i.e. $\sim 1\,\%$) and so is not discernible.

The scatter in these experimental results arises largely from errors in the mean field (which is difficult to measure accurately) and is transferred to the mean-square field which is obtained as the sum $\bar{\theta}^2 + \sigma_\theta^2$. The fluctuation field itself can be measured more accurately. Figure 8 shows measured and modelled vertical distributions of σ_θ normalized by the centreline value. The abscissa is normalized by the mean-field dispersion σ_m. There is an excellent correspondence between theory and experiment. Near the source, fluctuations are strongly peaked at $z/\sigma_m = 1$; that is, fluctuations are strongest where the gradient of the mean field is greatest. This is because near the source, fluctuations are produced mainly by bulk movement of the plume (meandering) with little contribution from structure within the plume (Uberoi & Corrsin 1953; Sawford 1983). With increasing distance downstream, this peak diminishes and moves towards the centreline until sufficiently far downstream a self-similar Gaussian form is approached. Warhaft (1984) found the off-centreline peak to re-emerge at $x_w/M = 63$, but this is not predicted by our model.

It is apparent from comparison of the results in figure 8 that theory and experiment are also in good quantitative agreement. This is confirmed by figure 9 which shows the peak value of $\sigma_\theta(z)/\sigma_\theta(0)$ as a function of x_w. The dashed line is the theoretical small-time limit derived from (3.8) and (3.9) using the result $s^2(0, t) \sim \frac{1}{2}\rho^2\sigma_z^4/\sigma_0^4$ (Sawford 1983), (which is valid for $\sigma_0^2 \gg \sigma_z^2$) with the small-time limits $\sigma_z^2 = 2\kappa t$, $\rho = \sigma_w^2 t^2$. There is generally good agreement between theory and experiment, although the peak fluctuations are increasingly underestimated as the source is approached. The reason for this is unclear but it seems likely that it is associated with our simplified treatment of source conditions and that, in practice, fluctuations which are generated in the boundary layer around the hot wire take some time to decay.

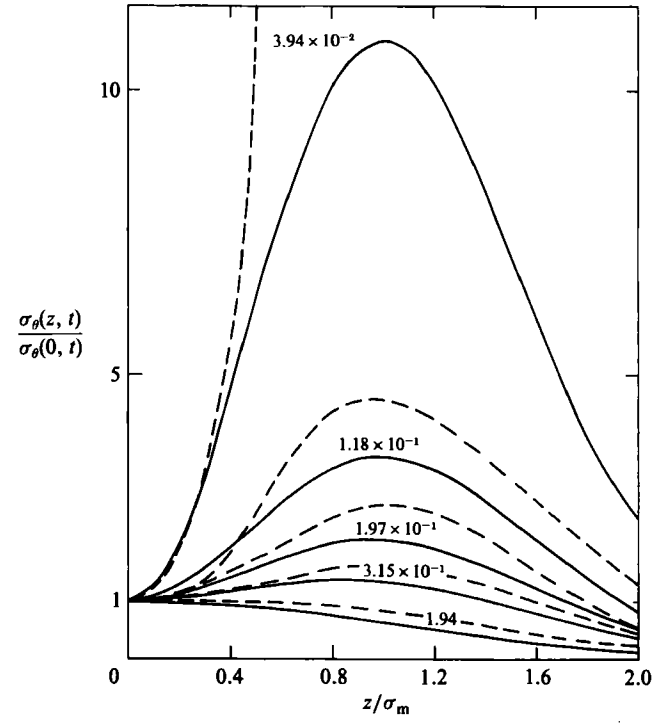

FIGURE 8. Model (——) and experimental (– – –) vertical distribution of the variance of the normalized temperature-fluctuation. Curves are labelled by x_w/M.

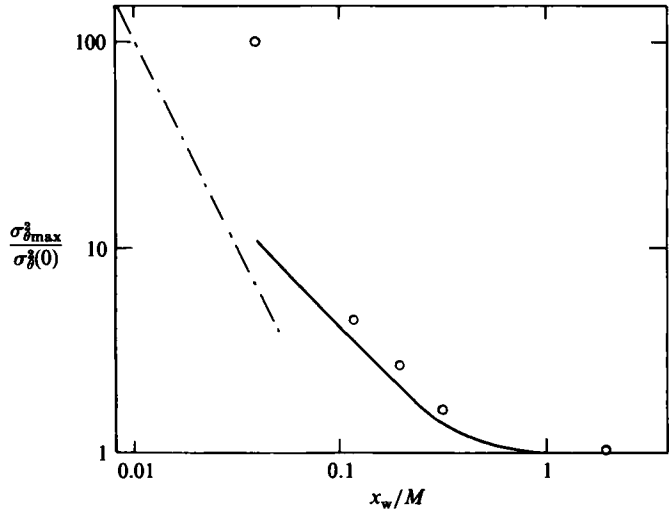

FIGURE 9. Ratio of peak-to-centreline variance of temperature fluctuations as a function of distance. Experiments (⊙); model (—); small-time limit for theory (– –).

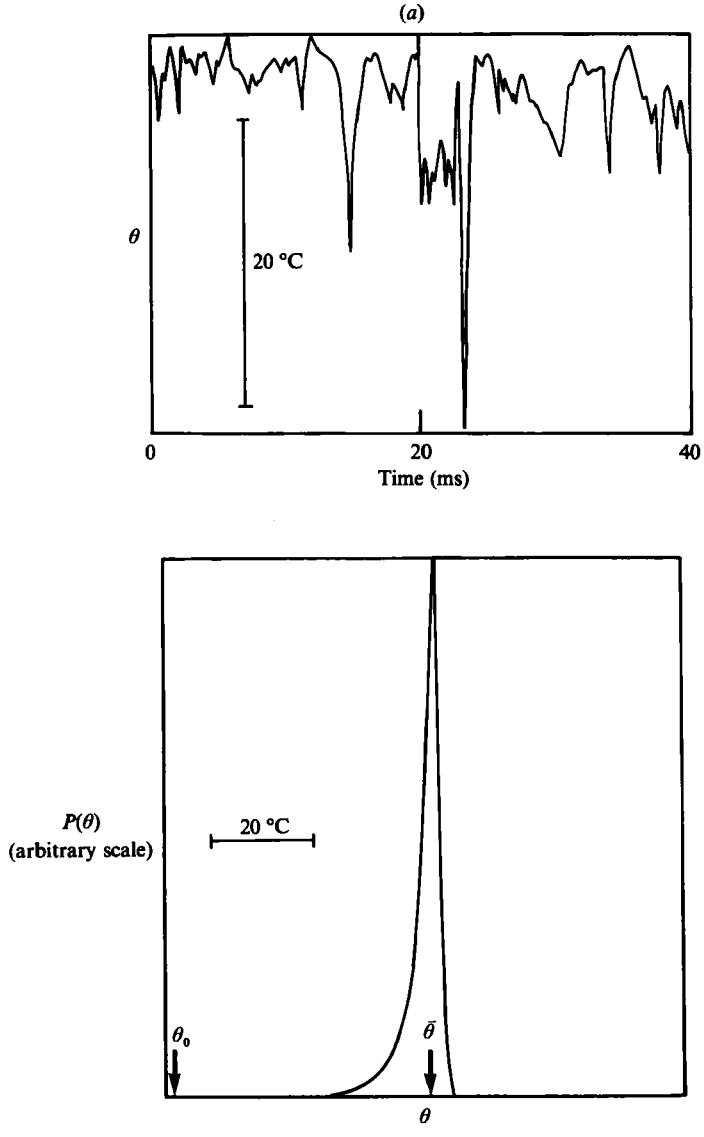

FIGURE 10(*a*). For caption see page 415.

4.3. *Streamwise development along the centreline*

4.3.1. *Temperature traces and frequency distributions*

Figure 10 shows temperature traces and temperature frequency distributions at three points on the plume centreline. Very close to the source ($x_w/M = 7.9 \times 10^{-2}$) the instantaneous plume width, σ_r (determined mainly by the source size and growth by molecular diffusion) is rather larger than σ_c, the standard deviation of the position of the centre-of-mass, which grows linearly with distance. Consequently, the temperature probe is immersed in hot air most of the time, only encounters cooler air occasionally and almost never comes into contact with, unheated air. Thus the frequency distribution peaks at high temperatures. The lack of structure *within* the instantaneous plume is clear from the very sharp cutoff in the hot side of the peak,

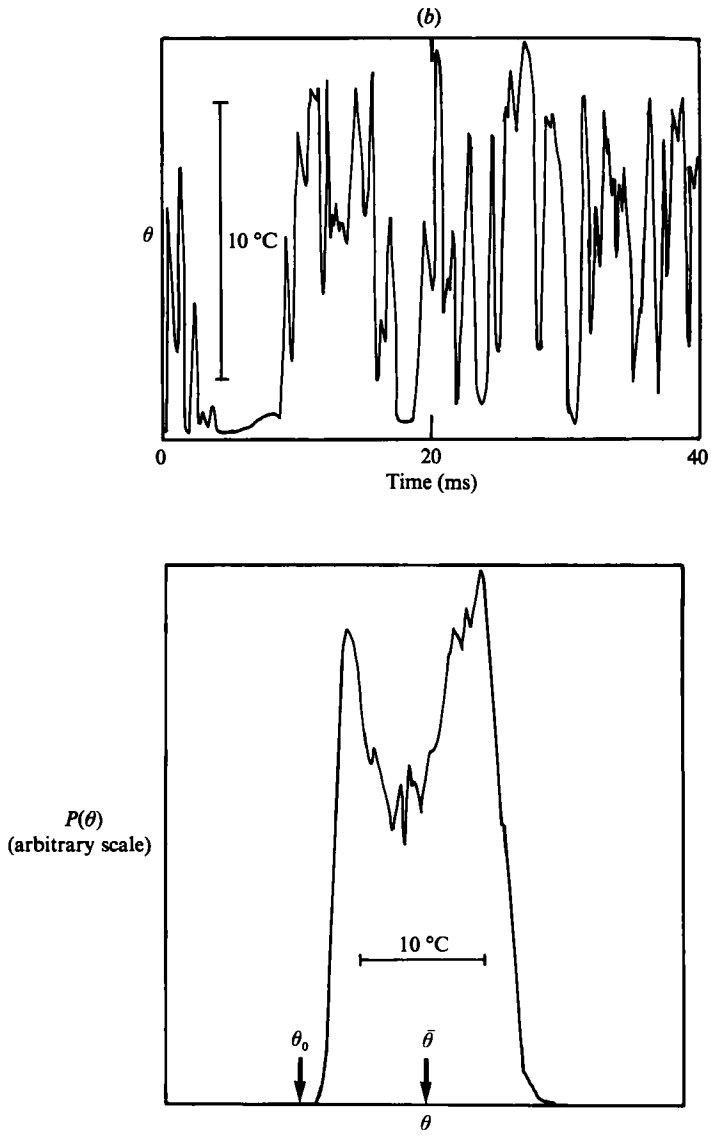

FIGURE 10(b). For caption see facing page.

indicating a well-defined, nearly constant peak temperature at the centre of the instantaneous plume.

Further downstream ($x_w/M = 0.63$) σ_r and σ_c are about equal and centre-of-mass motions cause the probe to sample the whole of the instantaneous plume from the hot centre to the unheated air beyond its edge, and in fact the probe spends significant periods in unheated air. Because the temperature distribution within the instantaneous plume is fairly flat in the centre, with a rapid drop to the background temperature outside the plume, the temperature trace shows rapid transitions from hot to cold as the plume swings back and forth. This feature shows up in the frequency distribution as a double peak – the probe spends most of the time in hot or cold air and less time in warm air. However, the high temperatures are more variable and the cutoff in the high-temperature peak is not as sharp as it was closer to the source.

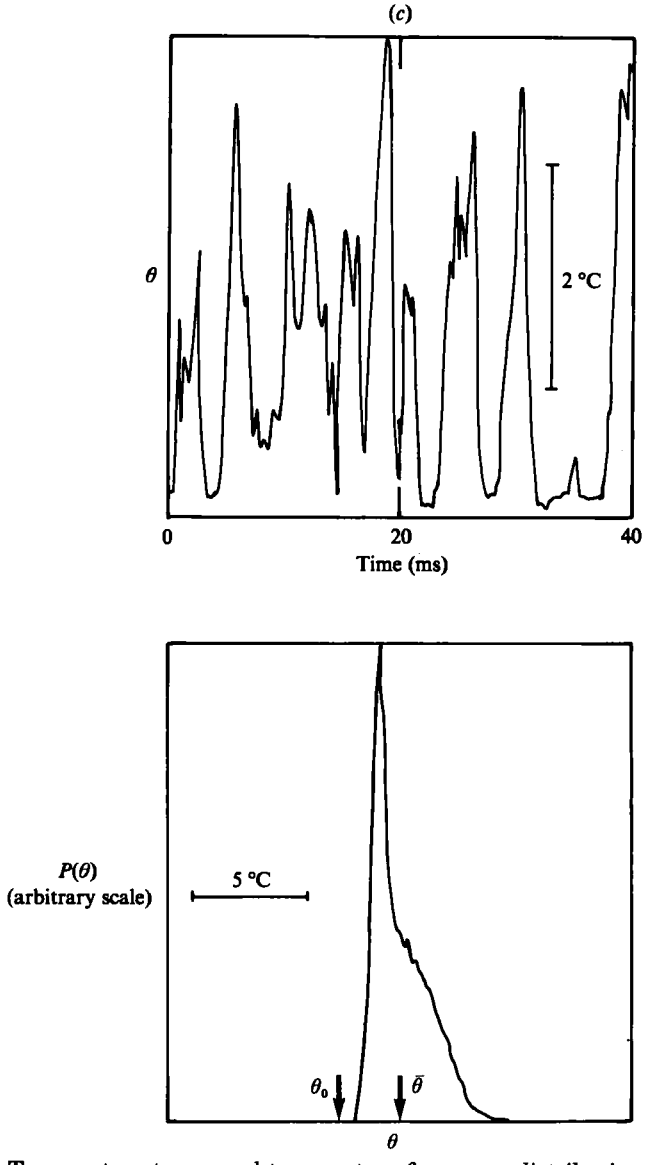

FIGURE 10. Temperature traces and temperature frequency distributions on the plume centreline at (*a*) $x_w/M = 7.9 \times 10^{-2}$, (*b*) 6.3×10^{-1}, (*c*) 3.9. Mean temperature $\bar{\theta}$ and background air temperature θ_0 are indicated.

Thus although at this point meandering is a very important (and indeeed the dominant) mechanism for generating concentration fluctuations, there is no longer a well-defined, nearly constant temperature at the centre of the instantaneous plume, and internal structure of the instantaneous plume is becoming apparent.

At $x_w/M = 3.9$, $\sigma_c \approx 2\sigma_r$. The temperature trace now shows substantial periods when the probe is in unheated air and this 'intermittency' is manifested as a sharp cold-side cut-off to the frequency distribution. However, the signal no longer shows the sharp transitions from hot to cold and there is no high-temperature peak in the frequency distribution. Clearly now temperature fluctuations are comparable with mean temperatures *within* the instantaneous plume. Nevertheless, meandering still

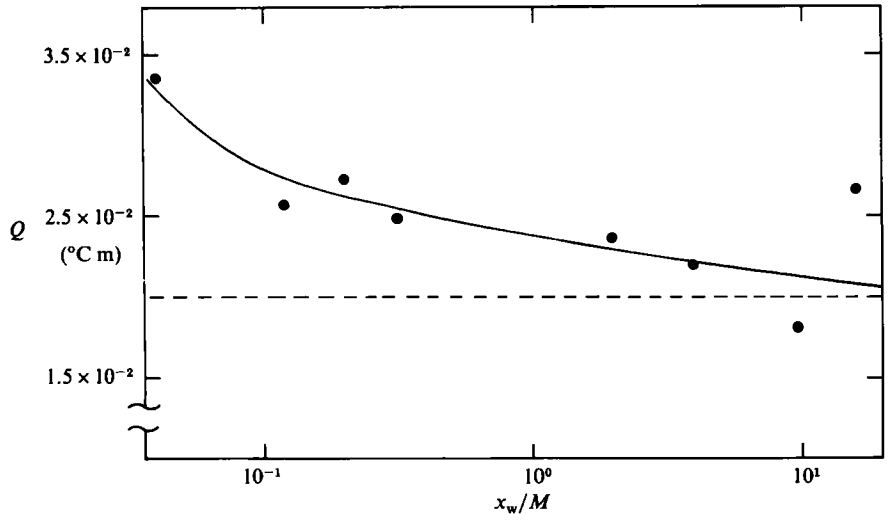

FIGURE 11. Effective source strength, $Q = \int \bar{\theta}\, dz$ as a function of x_w/M. Experiments (●); fit by eye (—); nominal source strength for heating rate of 105 W m^{-1} and air at 30 °C (– –).

makes a significant contribution to fluctuations at a fixed point. Indeed for the approximately self-similar asymptotic stage of growth for $t \gg t_L(0)$ a persistent residual contribution to fluctuations by meandering is to be expected since then the turbulence lengthscale L and the plume length-scales σ_m and σ_s all grow at the same rate and there will always be a proportion of turbulence kinetic energy on scales larger than the plume. However, the level of intermittency in Uberoi and Corrsin's (1953) Figure 11 for $x_w/M = 40$ suggests that this residual meandering contribution to fluctuations is not large.

4.3.2. *Effective source strength*

Figure 11 shows the effective source strength, $Q = \int_{-\infty}^{\infty} \bar{\theta}\, dz$ as a function of x_w. The points have been calculated from the least-squares parameters obtained by fitting Gaussians to the mean-temperature profiles, i.e. $Q = (2\pi)^{\frac{1}{2}} \bar{\theta}(0, x_w)\sigma_m$. The solid line has been drawn by eye. The scatter is mainly due to scatter in σ_m. Also shown, as the dashed line, is the nominal source strength, $H/(\rho_a\, UC_p)$, where ρ_a is the density and C_p the heat capacity at constant pressure of the air, calculated from the measured power input into the wire ($H = 105$ W m^{-1}) using air properties at 30 °C ($\rho_a\, C_p = 1.16 \times 10^3$ J m^{-3} K^{-1}). Clearly the effective heat content is greater than that calculated at room temperature, as a result of the combined effects of the velocity defect in the mean motion behind the wire and the modified air properties at the higher temperatures near the wire and in the plume.

4.3.3 *Mean temperature*

The mean temperature on the plume centreline is shown as a function of x_w in figure 12. The solid line has been calculated from our model, using the effective source strength shown in figure 11.

Figure 12 also shows (the broken line) the mean temperature calculated from Durbin's (1980) model for the motion of marked fluid elements. Molecular processes,

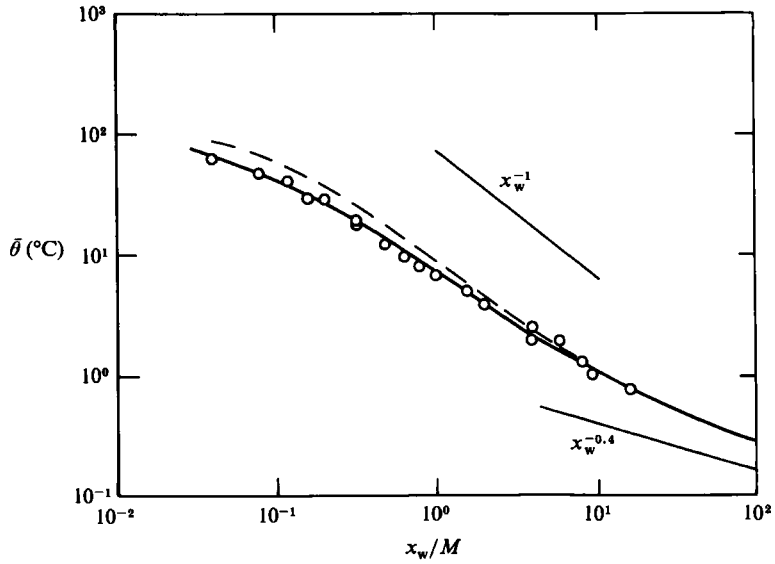

FIGURE 12. Mean temperature on plume centreline. Experiments (○); model results including molecular diffusion and viscosity for $\sigma_0 = 0.92\, d_w$ (——); model results without molecular processes $\sigma_0 = 0.92\, d_w$ (– – – –).

which are not explicitly included in this model, clearly have a large influence on the mean temperature only near the source where the plume is very narrow.

In general figure 12 reflects the relationship (3.8) between the width of the mean plume, σ_m (see figure 7) and the mean temperature and reinforces our earlier conclusions concerning the variation of σ_m with distance. Near the source where σ_m is dominated by the source size, σ_0, $\bar{\theta}$ changes only slowly with distance. Further downstream $\bar{\theta}$ decreases as x_w^{-1}, corresponding to the linear growth regime in σ_m. Asymptotically, the rate of decrease of $\bar{\theta}$ is consistent with the approach to a $x_w^{0.4}$ growth by σ_m, but this stage was not really reached in the experiments.

4.3.4. *Fluctuation variance and intensity*

Figure 13 shows σ_θ as a function of x_w (or travel time) on the plume centreline. Close to the source, fluctuations increase strongly with x_w, reaching a maximum at about $0.2M$ and then decreasing monotonically.

The data do not extend sufficiently far downstream to conclusively test the large-time theoretical prediction, $\sigma_\theta \sim \sigma_m^{-1} \sim x_w^{-0.4}$. They appear to be falling off more rapidly than this but this impression is strongly dependent on the most downstream point. Model predictions using the effective source strength of figure 11 are shown by the solid line and agree with the data to within about a factor of two over much of the range considered. Agreement deteriorates very close to the source (recall also figure 9 and the associated discussion) and, less dramatically, at the downstream extremity of the data. The model prediction is consistent with the $x_w^{-0.4}$ asymptote. The timescale on which σ_θ evolves (e.g. the location of the peak) is predicted very well.

Figure 13 also shows (as broken lines) predictions of Durbin's (1980) marked-particle model in which explicit molecular processes are ignored. For $\sigma_0 = 1.4 \times 10^{-4}$ m (the same as that used in our extended model) the marked-particle model overpredicts by nearly an order of magnitude but accurately predicts the location of the peak.

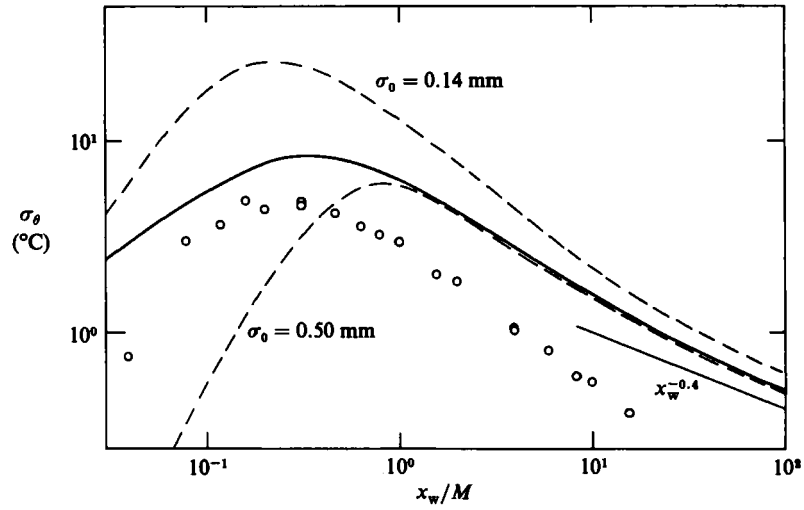

FIGURE 13. Standard deviation of temperature fluctuations on plume centreline. Experiments and model results including molecular processes as in figure 12. Model results without molecular processes are labelled according to source size.

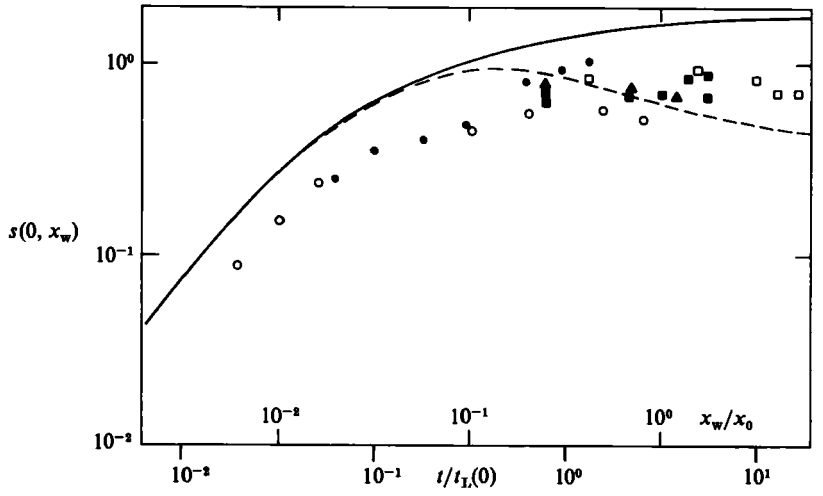

FIGURE 14. Intensity of temperature fluctuation. Experiments: present data, $d_w = 0.152$ mm (○); Warhaft (1984), $d_w = 0.127$ mm (□); $d_w = 0.025$ mm (●); Uberoi & Corrsin (1953), $d_w = 0.203$ mm (■); Townsend (1954), $d_w = 0.025$ mm (▲). Model results including molecular effects (——); meandering contribution (– – –).

Clearly, explicit molecular effects are very important. Arbitrarily increasing the source size improves the marked-particle-model prediction of the magnitude of σ_θ, but at the expense of moving the peak downstream. It is not possible to match both the magnitude and location of the peak without treating molecular processes explicitly.

The intensity of fluctuations, $s = \sigma_\theta/\bar{\theta}$, is shown as a function of x_w/x_0 and $t/t_L(0)$ in figure 14. There are two reasons for plotting the data in this way. First, the dependence on source strength is eliminated which facilitates comparison with other

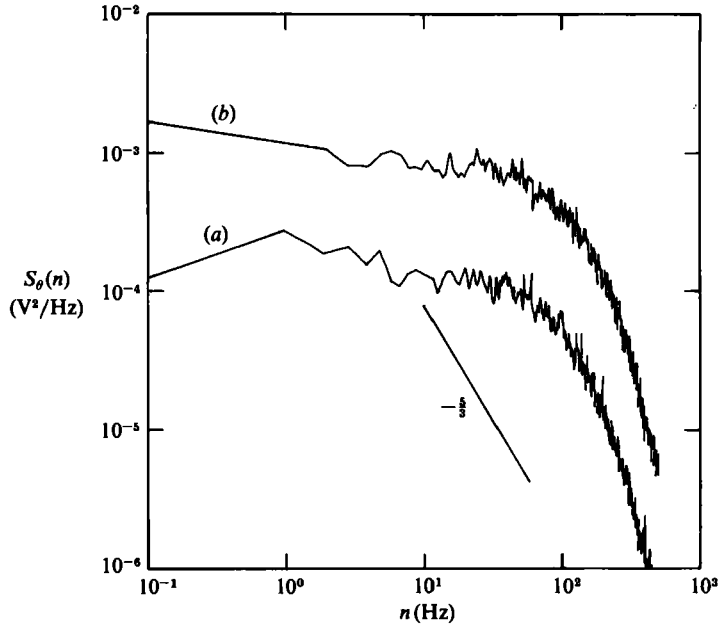

FIGURE 15. Temperature spectra on the plume centreline at (*a*) $x_w/M = 3.94 \times 10^{-2}$; (*b*) 9.65

work. Secondly, the magnitude of the fluctuations relative to the mean field is of interest in its own right as an indication of structure within the plume.

The measured intensity of fluctuations increases rapidly near the source before flattening out rather quickly at a level of about 0.6 further downstream. The experiments of Townsend (1954). Uberoi & Corrsin (1953) and Warhaft (1984) under similar conditions ($d_w \leqq \eta$; $Re \approx 100$) show comparable but larger fluctuation intensities with considerable scatter. Again our model results (solid line) reproduce these data to within about a factor of two.

The dashed line is the meandering contribution to the intensity of fluctuations. It peaks at about $x_w/x_0 = 0.1$ and decreases thereafter, with a tendency towards a constant value of about 0.4 in the approximately self-similar asymptotic stage beyond $x_w/x_0 \sim 2$. There the model predicts that meandering contributes only about 5% of the fluctuation variance and the intensity of fluctuations is dominated by internal structure or patchiness within the plume. This is consistent with the small degree of intermittency observed by Uberoi & Corrsin (1953) in temperature traces in this stage of plume development (see also §4.3.1)).

4.3.5. *Spectra and lengthscales*

Figure 15 shows fixed-point temperature spectra on the plume centreline very close to the source ($x_w/M = 3.94 \times 10^{-2}$) and well downstream ($x_w/M = 9.65$). Neither spectrum shows an extensive ($-\frac{5}{3}$) inertial subrange and it is apparent that the scale of the temperature fluctuations is larger at the downstream station. Lengthscales estimated from spectra at a range of downstream positions by extrapolating to the zero-frequency limit $S_\theta(0) = \overline{\theta'^2}\, L_\theta^{(x)}/U$ are shown in figure 16(*a*). There is considerable scatter, but the striking feature is the lack of a trend for $x_w/M < 5$, with a value of $L_\theta^{(x)}/M$ between 0.15 and 0.3 being representative. This feature was confirmed by analysis of the time correlation function for temperature fluctuations,

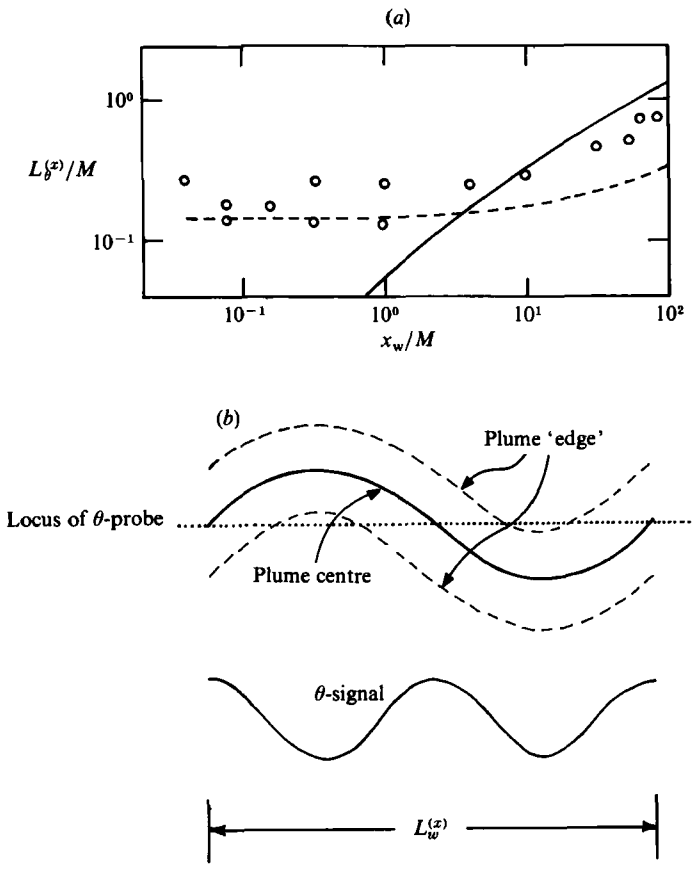

FIGURE 16. (*a*) Longitudinal lengthscale of temperature fluctuations on the plume centreline (○). The lines are: ---, $\frac{1}{2} L_x^{(w)}$; ——, σ_m (*b*) Schematic showing the relationship between the lengthscale of temperature fluctuations and the turbulence lengthscale for a meandering plume.

which also showed no trend over this range of distances and gave an average timescale of 1.3 ms corresponding to $L_\theta^{(x)}/M = 0.22$. Figure 16(*a*) also compares $L_\theta^{(x)}$ with the lengthscale of the velocity fluctuations, $L_\theta^{(x)}$ ($\frac{1}{2}L_w^{(x)}$ is plotted as a dashed line) and the half width of the mean plume σ_m, which is shown as the full line. Near the source, $L_\theta^{(x)} = \frac{1}{2}L_w^{(w)}$. This is consistent with the physical picture of a sinuous plume of mean wavelength $L_w^{(x)}$ being advected past the measurement point with velocity U. For a point on the mean plume centreline such a model gives $L_\theta^{(x)} = \frac{1}{2}L_w^{(x)}$, since on each 'wave' the measurement point traverses the plume twice (see figure 16*b*). Far downstream, $L_\theta^{(x)}$ appears to be more closely related to σ_m as would be expected for a plume developing in a self-similar way.

4.4 *Vortex shedding at* $Re_w \sim 200$

A few experiments were conducted with a thicker wire ($d_w = 0.711$ mm; $Re_w \approx 200$ for air at 30 °C) in order to assess the influence of vortex shedding on the temperature field. Figure 17 shows temperature spectra on the centreline downstream of the wire. Peaks at the vortex-shedding frequency, $0.2\,U/d_w$ and at its first harmonic have significant amplitudes close to the source wire ($x_w/M = 7.9 \times 10^{-2}$), but are much weaker at $x_w/M = 0.79$.

Figure 18 shows $\bar{\theta}$ and $\overline{\theta^2}$ as functions of x_w. The data have been normalized by

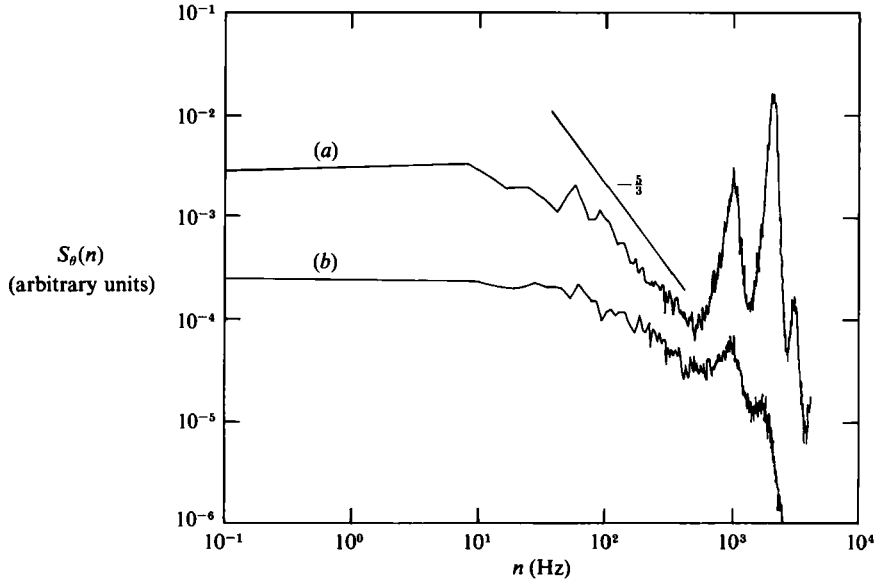

FIGURE 17. The effect of vortex shedding on the spectrum of temperature fluctuations on the plume centreline.

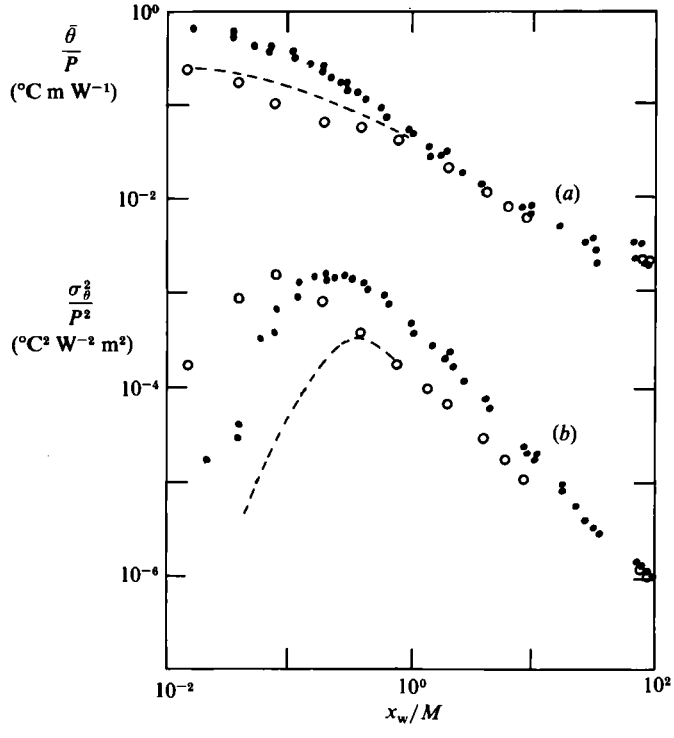

FIGURE 18. The effect of vortex shedding on (*a*) the mean temperature, and (*b*) the variance of temperature fluctuations on the plume centreline. Experiments: ●, without vortex shedding ($d_w = 0.152$ mm); ○, with vortex shedding ($d_w = 0.711$; $Re_w \approx 200$). The dashed line gives an indication of the results which would be obtained for the thicker wire without vortex shedding.

the power supplied to the wire and can thus be compared directly with similarly normalized data for the thinner source wire ($d_w = 0.152$ mm) which are also shown.

Immediately downstream of the source, $\bar{\theta}$ is lower for the thicker wire, as is expected since a greater volume of air is heated. However, the formation of the vortex street breaks up the heated wake into streaks of hot fluid. At the same time, in the first ten or so wire diameters downstream, the envelope of the vortices grows more rapidly than does the mean plume width at the turbulence levels encountered in these experiments. Thus in a *time-averaged* sense the hot air is spread over greater distances by vortex shedding although the *instantaneous* distribution is more concentrated. Compared with a turbulent plume from the same wire, the vortex street produces a lower mean temperature and higher fluctuations about the mean.

These features are apparent in figure 17. The dashed lines have been sketched to indicate the anticipated variation with x_w for a turbulent plume from a wire of the same size. They are not meant to be quantitative but rather to emphasise in a qualitative way the effect of vortex shedding. As a result of vortex shedding, the mean temperature is reduced for distances up to about $30\,d_w$, which is also roughly the point at which the vortex-shedding peaks disappear from the spectrum (see figure 15). Beyond this point the mean temperature is also indistinguishable from that due to the thinner wire.

Figure 18(*b*) shows that, compared with the turbulent plume from the thinner wire, vortex shedding produces a slightly larger peak in temperature fluctuations which also occurs nearer to the source. For turbulent plumes the opposite is true; a larger source results in a lower peak further downstream as indicated by the dashed line (see also the model results in figure 13). There is no clear indication from figure 18 of the point where vortex shedding ceases to influence σ_θ^2, but the spectral data indicated that it is unimportant beyond $x_w/M \sim 1$ or about $30\,d_w$. Still further downstream σ_θ^2 approaches that due to the thinner wire.

5. Conclusions

We have examined in detail, both experimentally and theoretically, the structure and development of the plume behind a line source in homogeneous turbulence.

A wide range of experimental evidence based on direct examination of the temperature traces, on frequency distributions, spectra and lengthscales of the temperature fluctuations and on the downstream evolution of the intensity and spatial distribution of fluctuations confirms the physical picture for the development of plumes that we foreshadowed in the Introduction and which is illustrated schematically in figure 19.

The plume begins as an instantaneously smooth distribution of material which near the source flaps about only slightly. With increasing distance downstream, the instantaneous plume width grows more slowly than the mean width and the meandering motion of the plume increases. As observed in absolute coordinates this increasing meandering motion dominates the concentration fluctuations for travel times from the source of $O(t_L)$. But near the centre of plumes from small sources, meander only determines σ_θ for periods somewhat less than t_L (SH). The intensity of fluctuations increases rapidly throughout this phase and the lengthscale of fluctuations is closely related to the lengthscale of the turbulence.

The instantaneous plume also develops increasing structure throughout this phase so that the distribution of tracer material within the plume becomes increasingly patchy. Sufficiently far downstream (many t_L) this patchiness within the plume

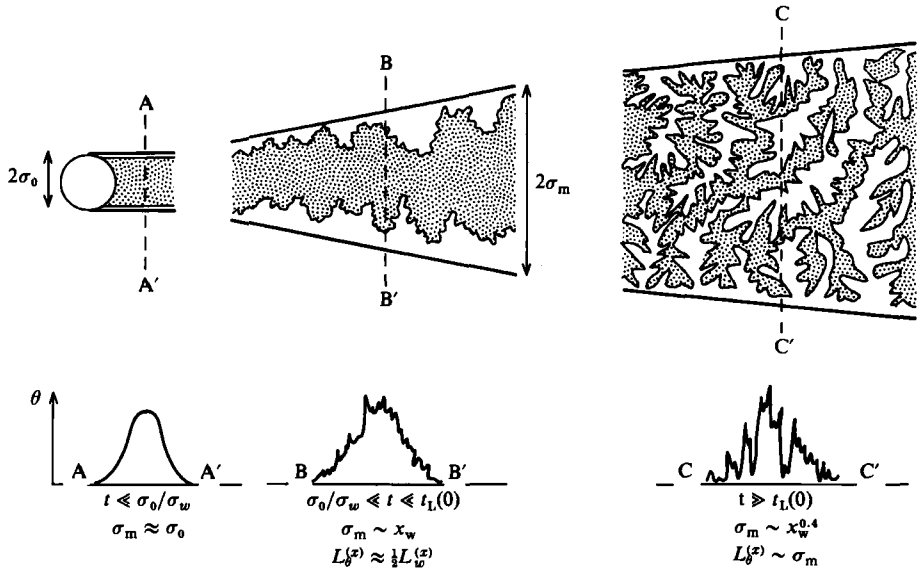

FIGURE 19. Schematic of the development of structure and concentration fluctuations in a turbulent plume.

dominates the concentration fluctuations and the plume develops in a self-similar manner in which the intensity of fluctuations is constant and spatial properties (including the lengthscale of fluctuations, the instantaneous plume width and the width of the mean-square plume) scale with σ_m, the half-width of the mean-concentration distribution. However, even in the meander-dominated stage of the plume, the developing patchiness plays an important role in mixing between plume and background materials and, for example, in chemical reactions.

The stochastic model of Durbin (1980) (modified by SH) accounts for a wide range of the measured properties of the temperature field of the plume and provides a unified treatment of all stages of plume development. On the scale of these laboratory measurements, molecular diffusion and viscosity have an important influence on concentration fluctuations, not just near the source where the plume is narrow, but everywhere. Although our representation of these molecular processes is quite crude, the model quantitatively predicts many detailed features of the temperature field. No doubt some tuning (e.g. by adjusting the parameter α in the uniform-strain model) would produce a better fit to the data, but this was not our aim. We were chiefly concerned to show how molecular processes affect fluctuations and what features are most influenced. We found that the magnitude and intensity of fluctuations are most influenced and that spatial properties of the distribution of fluctuations are much less sensitive.

Including the data of Townsend (1954) and Uberoi & Corrsin (1953), and Warhaft (1984), the asymptotic intensity of fluctuations is scattered over a range of 0.6–1.0 for wires ranging from 0.025 to 0.711 mm in diameter but there is no consistent trend with source size.

H. S. and B. L. S. acknowledge support by SERC and NERC, respectively, for their work done at Cambridge.

REFERENCES

BATCHELOR, G. K. 1982 Diffusion in a field of homogeneous turbulence. II. The relative motion of particles. *Proc. Camb. Phil. Soc.* **48**, 345–362.

BRAY, K. N. C. 1980 Turbulent flows with premixed reactants. In *Turbulent Reacting Flows* ed. P. A. Libby & P. A. Williams. Springer.

CORRSIN, S. 1952 Heat transfer in isotropic turbulence. *J. Appl. Phys.* **23**, 113–118.

CSANADY, G. T. 1973 *Turbulent Diffusion in the Environment*. Reidel.

DURBIN, P. A. 1980 A stochastic model of two-particle dispersion and concentration fluctuations in homogeneous turbulence. *J. Fluid Mech.* **100**, 279–302.

DURBIN, P. A. 1982 Analysis of the decay of temperature fluctuations in isotropic turbulence. *Phys. Fluids* **25**, 1328–1332.

FACKRELL, J. R. & ROBINS, A. G. 1982 Concentration fluctuations and fluxes in plumes from point sources in a turbulent boundary layer. *J. Fluid Mech.* **117**, 1–26.

GIFFORD, F. 1960 Peak to average concentration ratios according to a fluctuating plume dispersion model *Intl. J. Air Poll.* **3**, 253–260.

HINZE, J. O. 1975 *Turbulence*, 2nd edn. McGraw Hill.

HUNT, J. C. R. 1976 Air Pollution Dispersion. Film PT272/07 and Programme notes made with BBC for Open University Course on Environmental Control and Public Health.

JONES, C. D. 1982 On the structure of instantaneous plumes in the atmosphere. *J. Hazardous Materials* **7**, 87–112.

LAMB, R. G. 1981 A scheme for simulating particle-pair motions in turbulent fluid. *J. Comput. Phys.* **39**, 329–346.

MONIN, A. S. & YAGLOM, A. M. 1971 *Statistical Fluid Mechanics: Mechanics of Turbulence*, volume 1. MIT Press.

MONIN, A. S. & YAGLOM, A. M. 1975 *Statistical Fluid Mechanics: Mechanics of Turbulence*, volume 2. MIT Press.

POPE, S. B. 1979 The statistical theory of turbulent flames. *Phil Trans. R. Soc. Lond* A **291**, 529–568.

SAFFMAN, P. G. 1960 On the effect of molecular diffusivity in turbulent diffusion. *J. Fluid Mech.* **8**, 273–283.

SAWFORD, B. L. 1983 The effect of Gaussian particle-pair distribution functions in the statistical theory of concentration fluctuations in homogeneous turbulence. *Q. J. R. Met. Soc.* **109**, 339–354.

SAWFORD, B. L. 1984 Reply to comments by Egbert and Baker on 'The effect of Gaussian particle-pair distribution functions in the statistical theory of relative dispersion. *Quart. J. Roy. Met. Soc.* **109**, 339–354'. *Quart. J. Roy, Met. Soc.* **110**, 1199–1200.

SAWFORD, B. L. & HUNT, J. C. R. 1986 Effects of turbulence structure, molecular diffusion and source size on scalar fluctuations in homogeneous turbulence. *J. Fluid Mech.* **165**, 373–400.

SCHLICHTLING, H. 1968 *Boundary Layer Theory*, 6th Edn. Pergamon.

SNYDER, W. H. & LUMLEY, J. L. 1971 Some measurements of particle velocity auto-correlation functions in a turbulent flow. *J. Fluid Mech.* **48**, 41–71.

SREENIVASAN, K. R., TAVOULARIS, S., HENRY, R. & CORRSIN, S. 1980 Temperature fluctuations in grid-generated turbulence. *J. Fluid Mech.* **100**, 597–623.

TAYLOR, G. I. 1921 Diffusion by continuous movements. *Proc. Lond. Math. Soc.* **20**, 196–212.

TOWNSEND, A. A. 1954 The diffusion behind a line source in homogeneous turbulence. *Proc. R. Soc. Lond.* A **224**, 487–512.

UBEROI, M. S. & CORRSIN, S. 1953 Diffusion of heat from a line source in isotropic turbulence. *NACA Rep.* 1142.

WARHAFT, Z. 1984 The interference of thermal fields from line sources in grid turbulence *J. Fluid Mech.* **144**, 363–387.

WARHAFT, Z. & LUMLEY, J. L. 1978 An experimental study of the decay of temperature fluctuations in grid-generated turbulence. *J. Fluid Mech.* **88**, 659–684.

WYNGAARD, J. C. 1971 Spatial resolution of a resistance wire temperature sensor. *Phys. Fluids* **14**, 2052–2054.